

## ANALYSIS OF INTENSIVELY BLASTED ELECTRIC ARC BURNING IN THE ARC HEATER'S ANODE CHANNEL

J. SENK\*, I. JAKUBOVA, I. LAZNICKOVA

*Faculty of Electrical Engineering and Communication, BUT, Technicka 12, 616 00 Brno, Czech Republic*

\* corresponding author: [senk@feec.vutbr.cz](mailto:senk@feec.vutbr.cz)

**ABSTRACT.** The paper deals with the description of the intensively blasted electric arc burning in Ar in the anode channel of the arc heater operated under various conditions. Directly measured experimental data (current, voltage, gas flow rate, power loss) characterize the operation of the device as a whole, but important parameters describing the electric arc inside (its geometry, temperature and voltage distribution) must be revealed using a mathematical model of the arc. An updated version of the model is introduced and used for analysis of two exemplary sets of measured data. The results are given in figures and commented.

**KEYWORDS:** electric arc; arc heater; argon; modelling.

### 1. INTRODUCTION

A modular-type arc heater with the electric arc burning in a cylindrical anode channel, being cooled and stabilized by gas flow, was designed by the authors and experimentally operated under various operational conditions [1].

Various technological applications have been tested (e.g. decomposition of stable harmful substances, diamond deposition), and numerous data have been collected, which are useful e.g. in design, operation and usage of similar devices. The behaviour of the electric arc in the anode channel is of key importance for the operation of the device, but unfortunately substantial parameters of the arc cannot be observed and measured directly. The inner space of the device is inaccessible and basic properties of the arc are hidden in integral measured data. That is why a mathematical model of the arc has been designed which enables to determine the arc radius  $r_A$ , temperature  $T_A$  and voltage  $U_A$  distribution from the experimentally obtained integral data such as the total voltage  $U$  and current  $I$ , the gas flow rate  $Q_m$  and power loss  $P_l$  of individual segments of the arc heater determined by calorimetry.

During a long period of experiments and modelling, rather extent experience has been obtained and some previous assumptions have been modified. The basic laws and presumptions of the model [2] remain unchanged and are only briefly summarized in §2, which focuses mainly on new approaches in the new version of the model. Examples of computed dependences are given and discussed in §3. Finally, §4 concludes the paper.

In the paper, subscripts are used to define the part of the device or the arc itself. The arc heater is divided into several separately cooled segments which are chosen with respect to their expected power loss load and mechanisms of energy exchange between the arc and the segment in question. The following nota-

tion is used: In the downstream direction, subscript “cat” stands for the cathode, subscript “in” for the input part of the anode channel, subscript “ch” for the (anode) channel, and subscript “a” stands for the anode itself. Subscript “as” indicates the anode spot, the interface between the arc’s root and the grounded anode. Finally, subscript “A” means the arc.

### 2. MATHEMATICAL MODEL

The core part of the model describes the behaviour of the intensively blasted electric arc burning in the cylindrical anode channel of the arc heater. The model is based on the mass and energy conservation laws and Ohm’s law and altogether with the measured data it uses also transport and thermodynamic properties of working gas [3].

To make the text easy to read, the main assumptions are summarized here: the arc plasma is supposed to be in the local thermodynamic equilibrium, with its kinetic energy small compared to its enthalpy. Only the radial component of radiative energy flow and only the axial component of enthalpy flow are taken into account as predominant terms; the conductive heat loss of the arc is neglected based on previous experience. The cylindrical anode channel forces also the stabilized arc to be axially symmetrical. Mach number  $Ma$  is taken constant over the anode channel cross-section, i.e. the same in the hot arc zone and the cold surrounding zone. The development of the arc radius along the anode channel axis is assumed as follows:

$$r_A(z) = r_0 \left( 1 + \left( \frac{z}{r_0} \right)^{1/n_r} \right), \quad (1)$$

where  $r$  is the radius (m),  $z$  is the axial coordinate (m),  $n_r$  is the parameter to be found. As mentioned above, subscript A means the arc. Subscript 0 stands for the beginning  $z = 0$  at the cathode tip. The radius of the cathode spot  $r_0$  is determined from the

current density, which is supposed to be  $10^8 \text{ A m}^{-2}$  for currents up to 2.16 kA [4].

Previous experiments and computations have shown that using the rectangular temperature distribution across the anode channel is sufficient, which makes the computation much simpler  $T_A(r, z) = T_A(z)$ . Furthermore, in the cold zone between the arc and the anode channel wall the gas temperature has been found to be equal to its input temperature  $T_0$ .

The three basic integral equations are rewritten in the difference form and are solved in an equidistant mesh, with the exception of the beginning near the cathode tip. The total length of the arc  $z_L$  is divided into  $n$  steps  $\Delta z = z_L/n$ . Between adjacent segments, energy balance is assumed. In each slice ( $k = 1, 2, \dots, n$ ), the following equation system is solved:

- continuity equation

$$\text{Ma}(z_k) = \left( \pi(r_c^2 - r_A^2(z_k))\rho(T_0)a(T_0) + \pi r_A^2(z_k)\rho(T_A(z_k))a(T_A(z_k)) \right)^{-1} Q_m, \quad (2)$$

- energy equation

$$\pi r_A^2(z_k)\text{Ma}(z_k)\rho(T_A(z_k))a(T_A(z_k))h(T_A(z_k)) = (1 - p_1(z_L))U_A(z_k)I, \quad (3)$$

- Ohm's law

$$U_A(z_k) = U_A(z_1) + \frac{I}{\pi} \Delta z \sum_{j=2}^k \frac{1}{r_A^2(z_j)\sigma(T_A(z_j))}, \quad (4)$$

where — besides the quantities defined above —  $r_c$  is the anode channel radius,  $\sigma$  is conductivity,  $\rho$  density,  $a$  sound velocity,  $h$  enthalpy of the working gas,  $E(z)$  electric field intensity,  $Q_m$  is gas flow rate,  $\text{Ma}(z)$  Mach number. The loss coefficient  $p_1$  is the ratio of the total measured power loss reduced by the power loss of the cathode and the anode spot to the electric input power of the arc

$$p_1 = \frac{P_{1,\text{tot,meas}} - P_{1,\text{cat}} - P_{1,\text{as}}}{U_A(z_L)I}.$$

In the very first version of the model, only the behaviour of the electric arc was modelled and the influence of near-electrode regions was neglected. Later, the influence of the electrodes was included using the data given by other authors. In this new model, the near-electrode regions are included and solved using the real measured data.

The model describing the arc column is completed with calculations respecting special nature of the near-cathode and near-anode region. The treatment of these regions is in detail explained in [5] and acceptable agreement of obtained values with the data of other authors is found. Here, the solution of near-electrode regions is explained only in brief, with the

emphasis on implementation of these parts to the complex model. It should be stressed that although the near-electrode regions need a special approach, they cannot be calculated independently, but must be solved as a part of the whole calculation system altogether with the arc.

For near-electrode regions, first the power consumed in these regions must be estimated and then the total input power  $UI$  is split into three parts pertaining to the near-cathode region, the arc alone, and the near-anode region. In other words, only a part of the total voltage  $U$  pertains to the arc  $U = U_{\text{cat}} + U_A + U_{\text{as}}$ .

Thanks to the construction of the cathode and its shell and their intensive water cooling, the power consumed for building necessary conditions for the arc in the near-cathode region can be estimated in a simple way. It is measured separately as the power loss of the cathode  $P_{1,\text{cat}}$ . The corresponding cathode voltage drop is  $U_{\text{cat}} = P_{1,\text{cat}}/I$ . In the close vicinity of the cathode, in the near-cathode layer, non-equilibrium processes take place which are not studied here [6]. What is needed for further computation of the model of the arc is the distance from the cathode tip  $s$  and the corresponding temperature  $T_A(s)$  from which the axial arc development starts. For this purpose, the effective conductivity of the working gas  $\sigma[T_A(s)]$  is supposed to be corresponding to the cathode voltage drop  $U_{\text{cat}}$ , and the current density  $j(s)$  which is reached at the distance  $s$  from the cathode tip if the arc radius  $r_A(s)$  is taken from (1). Based on this consideration, the near-cathode layer width  $s$  can be determined from the following equation:

$$\sigma(T_A(s)) = \frac{j(0)}{(1 + (s/r_0)^{1/n_r})^2} \frac{s}{U_{\text{cat}}(I)}. \quad (5)$$

In this equation, first a suitable  $T_A(s)$  is chosen and the corresponding near-cathode layer width  $s$  is computed for the given  $n_r$ . It has been found that the selected temperature  $T_A(s)$  significantly affects the shape of the temperature distribution  $T_A(z)$  near the beginning, but soon its influence to  $T_A(z)$  dies down. Such a value of  $T_A(s)$  is used in further modelling which results in a fast and smooth increase of  $T_A(z)$  without extremes near the beginning. An accuracy of hundreds of kelvins is sufficient.

Obviously, the width of the near-cathode layer depends not only on the sort of the working gas, on the arc current  $I$  and the cathode voltage drop, but also on the exponent  $n_r$ , which describes the development of the arc radius along the  $z$  coordinate  $r_A(z)$ , see (1). This exponent is determined during the computation of the model as a whole as explained later.

In the near-anode region, the situation is more complicated, because the power consumed for the arc-anode attachment cannot be measured separately. In the anode, the arc is fully developed and the power irradiated from the arc column to the anode wall cannot be neglected or easily split off. For the first approximate estimation of the anode spot voltage

drop  $U_{as}$  the following consideration is used. The anode in the tested device has the same radius  $r_c$  as the anode channel but its length  $l_a$  is different than the length of the channel  $l_{ch}$ , here it was about three times shorter. Very steep changes in the arc radius and temperature take place especially near the beginning, while towards the end, both the radius and the temperature change more slowly. So it can be expected that near the end, the power transferred from the arc to the unit surface of the anode channel wall is roughly the same as that transferred to the unit surface of the anode wall. Then the separately measured power loss of the anode can be divided into the power obtained from the arc column and the power loss due to the arc/anode attachment  $P_{l,as}$ . Naturally, this first estimation of the anode spot power loss  ${}^0P_{l,as}$  and the corresponding anode spot voltage drop  ${}^0U_{as}$  is refined during iterative computation of the model as a whole.

The input data of the model are geometrical parameters of the device (radius and length of the input part of the anode channel  $r_{in}$ ,  $l_{in}$ , of the main part of the anode channel  $r_{ch}$ ,  $l_{ch}$ , of the anode  $r_a$ ,  $l_a$ ) and transport and thermodynamic properties of the working gas ( $\sigma$  is the conductivity,  $\rho$  density,  $a$  sound velocity,  $h$  enthalpy of the working gas) which are known before the experiment. Further set of input data is individually obtained for each experiment which is characterized by the current  $I$ , the total voltage  $U$ , gas flow rate  $Q_m$ , and measured power loss of individual segments of the device (power loss of the cathode  $P_{l,cat}$ , input part of the channel  $P_{l,in}$ , of the main part of the anode channel  $P_{l,ch}$ , and of the anode  $P_{l,a}$ ).

The computation starts with the above mentioned determination of the cathode voltage drop  $U_{cat}$  and the rough estimation of the anode spot voltage drop  ${}^0U_{as}$ . The arc voltage is  ${}^0U_A = U - U_{cat} - {}^0U_{as}$ . The first value of the exponent  $n_r$  is estimated from the energy balance at the output cross-section of the device at  $z = z_L$ . As mentioned above, the equation system (2)–(4) is solved in a mesh over the  $z$  axis. The step  $\Delta z$  of 1 mm is found to be suitable when the total length  $z_L$  is tens of millimetres (109 mm in the following examples). In the first node  $z_1$ , the first interval is of a different length ( $\Delta z - s$ ) than the others. Near the beginning, the electric field intensity falls very fast with the increasing distance from the cathode tip. To prevent overestimation of the voltage drop in the first interval, an average value of the computed electric field intensity is taken as an acceptable compromise

$$U_A(z_1) = \frac{\Delta z - s}{2\pi} \left( \frac{I}{r_A^2(s)\sigma(T_A(s))} + \frac{I}{r_A^2(z_1)\sigma(T_A(z_1))} \right). \quad (6)$$

Solving the equation system in the mesh step by step gives axial dependences of arc temperature  $T_A(z)$ ,

electric field intensity  $E(z)$ , Mach number  $Ma(z)$ , power loss  $P_l(z)$ , voltage  $U_A(z)$  and finally, at the end, the total arc voltage  $U_A(z_L)$  and  $P_l(z_L)$  as sums of individual increments. The calculation is repeated with slightly changed exponent  $n_r$  until the sum of the computed voltages for the  $i$ -th iteration  ${}^iU_A(z_L) + U_{cat} + {}^iU_{as}$  is (with an acceptable difference) equal to the total measured voltage  $U$ . Next, the estimation of the anode spot power loss must be refined first. Now not only measured power loss of the anode channel and the anode are available, but also the computed values obtained by summation within the  $k$ th iteration. They are mutually compared, and the estimation of the anode spot power loss is updated in the next step to better match the measured power loss of the channel and the anode.

The procedure is repeated until the difference between the two approaches starts to increase; the best approximation of the anode spot power loss is found.

After the calculation, the computed values of power loss and voltage distribution with acceptable errors correspond to the measured values. The next section illustrates some computations and gives examples of the axial dependence of the arc temperature and radius for the arc stabilized by argon of two different flow rates.

### 3. RESULTS AND DISCUSSION

The designed model of the arc including also its near-electrode regions was used for evaluation of two sets of experimental data. The arc heater with the channel radius  $r_c$  of 8 mm was operated on pure argon with two different flow rates (11.3 g/s and 22.5 g/s). The total distance from the cathode tip to the output of the anode  $z_L$  was 109 mm, consisting of the input part of the channel  $l_{in} = 22$  mm, the main part of the anode channel  $l_{ch} = 60$  mm, and the anode  $l_a = 27$  mm. The total input power  $P_{in} = UI$  was set approximately between 4 and 30 kilowatt.

In the following figures, if the figure compares the results obtained with both argon flow rates, solid symbols and lines are used for the lower flow rate of 11.3 g/s and empty symbols with dashed lines for the higher flow rate of 22.5 g/s.

Figure 1 compares the near-cathode layer width  $s$ , the corresponding arc temperature  $T_A(s)$  and the arc cross-section area  $S_A(s) = \pi r_A^2(s)$  at the distance  $s$  for two different argon flow rates and under different arc current  $I$ . Obviously, the increasing arc currents result in lower  $s$  and higher  $T_A(s)$ . As could be expected, for higher arc currents, the conditions for the arc burning are built in a closer vicinity of the cathode and the arc temperature is higher. For the same arc current, higher argon flow rate distinctly decreases the near cathode layer width and also the corresponding temperature is lower. The arc cross-section area is higher for the lower gas flow rate and higher arc currents, but it is worth mentioning that both the arc cross-section and the arc temperature cannot be directly compared

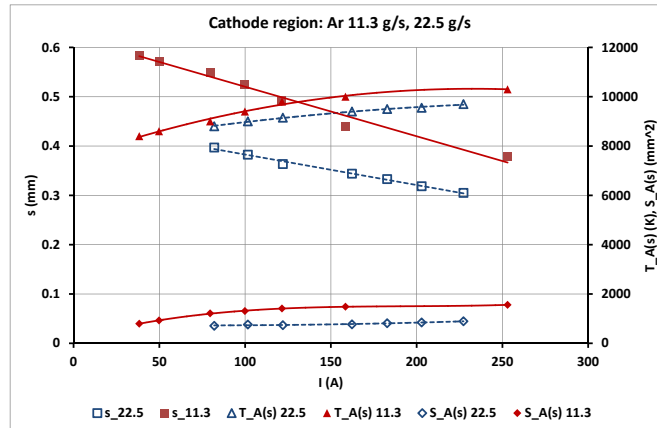


FIGURE 1. The near-cathode layer width  $s$ , the corresponding arc temperature  $T_A(s)$  and cross-section  $S_A(s)$  for two argon flow rates of 11.3 and 22.5 g/s.

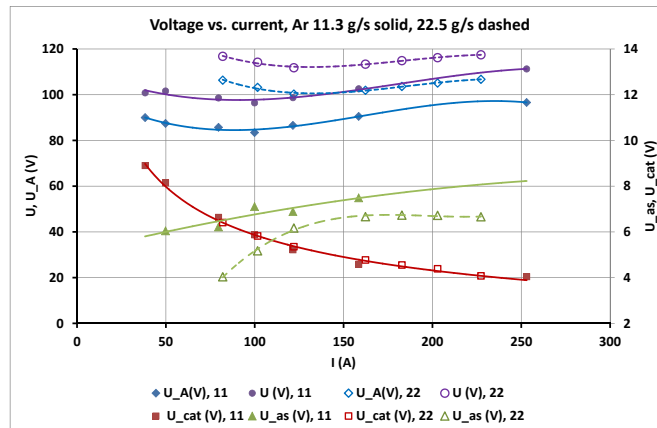


FIGURE 2. The voltage vs. current dependences for two argon flow rates 11.3 and 22.5 g/s: the measured voltage  $U$ , net arc voltage  $U_A$ , cathode voltage drop  $U_{cat}$ , and anode-spot voltage drop  $U_{as}$ .

between the two gas flow rates as they are reached at different distances  $s$  from the beginning.

Figure 2 gives the voltage vs. current dependences for both the investigated argon flow rates. The highest curves with circles are the measured total voltages  $U$ . As can be seen, the twice as high argon flow rate results in nearly by 10% higher total voltage. After computations, the net arc voltage  $U_A$  is obtained by subtracting the cathode voltage drop  $U_{cat}$  and the computed anode spot voltage drop  $U_{as}$  from the measured total voltage  $U$ . The dependences of the cathode and anode spot voltage drops on the arc current are given in the same figure and deserve a short notice. As observed in our older experiments, the cathode voltage drop does not depend on the gas flow rate at all and decreases with the increasing arc current. On the contrary, the anode spot voltage drops increase with the increasing arc current and

seem to exhibit some relationship to the gas flow rate. Higher argon flow rate results in a bit lower anode spot voltage drop. As a result of the opposite course of the cathode and anode spot voltage drop dependences on the current, their sum changes only little with the current and thus the shape of the curves  $U(I)$  and  $U_A(I)$  is almost the same, with the net arc voltage here being approximately by 10% lower than the corresponding measured total voltage  $U(I)$ . In both cases, the characteristics exhibit a typical S-shape with very slightly increasing voltage in the middle and slightly decreasing voltage at low (and probably also high) currents.

In Figures 3 and 4 typical computed axial dependences of the arc temperature  $T_A(z)$  and the arc radius  $r_A(z)$  are given for the argon flow rate of 22.5 g/s and several arc currents. It is clearly seen, that close to the beginning the arc temperature and the arc ra-

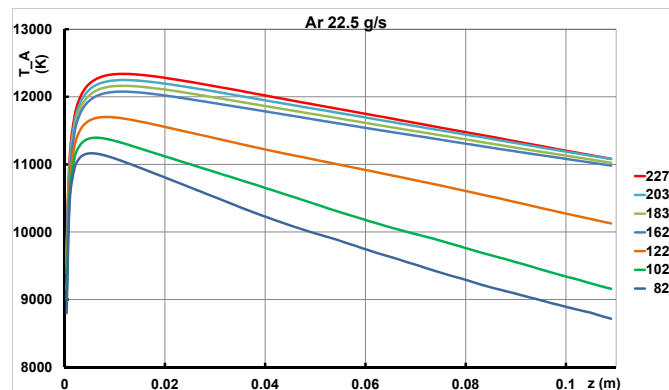


FIGURE 3. The computed distribution of the arc temperature on the channel axis  $T_A(z)$  for argon flow rate of 22.5g/s and different arc currents (the order of the legend items corresponds to the order of curves).

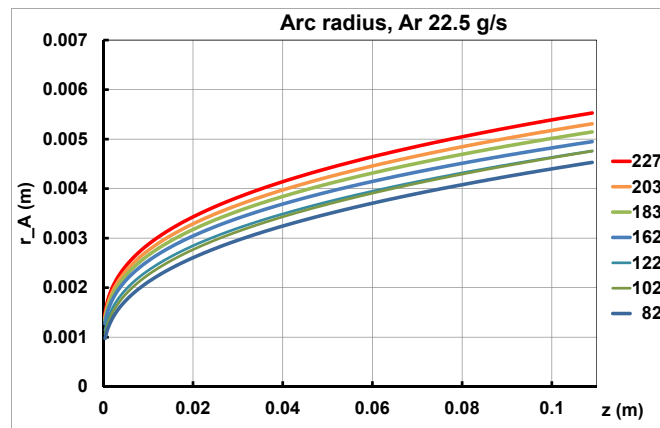


FIGURE 4. The computed distribution of the arc radius  $r_A(z)$  for argon flow rate of 22.5g/s and different arc currents (the order of the legend items corresponds to the order of curves at the channel).

dius quickly increase. While the arc radius increases along the whole channel (see (5)), the arc temperature begins to decrease soon. Steep changes of the arc temperature and radius in the input part of the anode channel (of the length of 22 mm in the discussed experiments) are the main reason why the input part is cooled separately and is not taken into account for estimation of the anode spot power loss. In the anode channel, the arc temperature decreases almost linearly with the increasing distance from the beginning. The legend in both figures gives the arc currents in the same order as the curves are at the end of the anode. Obviously, the output arc temperature  $T_A(z_L)$  first increases almost linearly with the arc current, but at higher currents this increase becomes slower and the output temperature does not increase any more.

In Figure 5 the computed arc temperature at the

end of the anode channel  $T_A(0.082 \text{ m})$  for argon flow rates of 11.3 g/s and 22.5 g/s is given in dependence on the total input power. Similarly, Figure 6 shows the computed arc cross-section at the end of the anode channel  $S_A(0.082 \text{ m})$  for both argon flow rates. It is clearly seen that the higher argon flow rate results in a smaller arc cross-section but a higher arc temperature. The arc column is narrow and hot which manifests in higher power irradiated to the channel walls. Also, the saturation of the arc temperature at higher currents at higher argon flow rate is apparent in Figure 5. Surprisingly, no similar saturation is seen at the arc temperature dependence for the half argon flow rate of 11.3 g/s. With this lower argon flow rate, both arc temperature and arc cross-section increase almost linearly with the input power within the tested range. Undoubtedly, a small slowdown can be observed at higher input power.

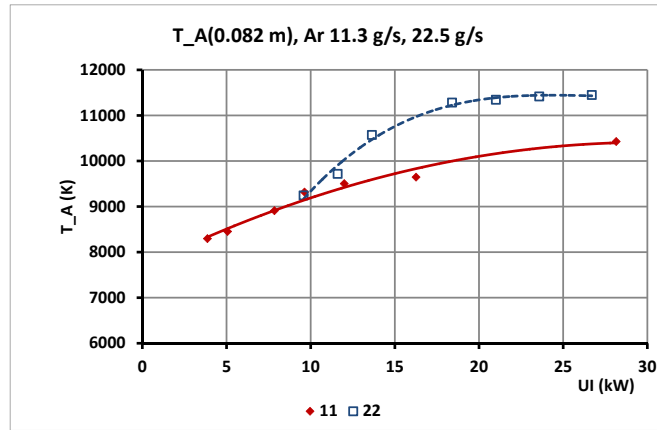


FIGURE 5. The computed arc temperature at the end of the anode channel  $T_A(0.082\text{ m})$  for argon flow rates of 11.3g/s (solid line, solid symbols) and 22.5 g/s (dashed line, empty symbols) vs. the total input power.

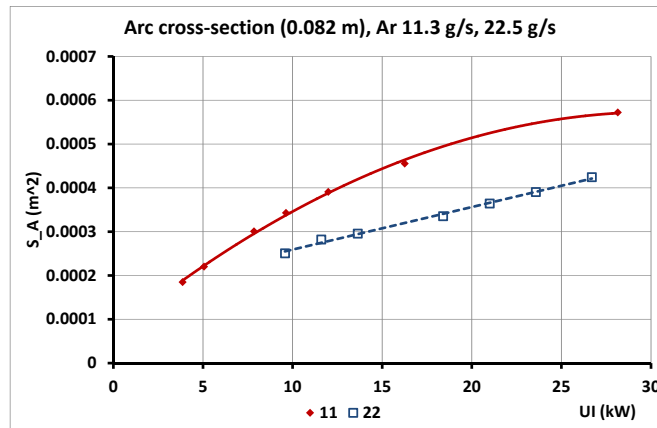


FIGURE 6. The computed arc cross-section at the end of the anode channel  $S_A(0.082\text{ m})$  for argon flow rates of 11.3g/s (solid line, solid symbols) and 22.5 g/s (dashed line, empty symbols) vs. the total input power.

#### 4. CONCLUSIONS

The paper introduces an updated model of the electric arc burning in the anode channel of the arc heater. The mathematical model not only describes the behaviour of the intensively blasted arc column but also enables to solve the problem of near-electrode regions in direct connection to the measured data obtained from the analysed experiment. The model is applied for analysis of two sets of experiments carried out under different argon flow rates. Selected results are illustrated in figures and reveal interesting observations. In the described cases, the difference between the computed (summed) arc voltage and the value determined from measured data was below one percent. Unfortunately, much higher error was observed with the computed and measured power loss of the anode, especially in some experiments. Probably, more precise method for determination of the anode spot

power loss should be sought for. Further experimental and computational experience may inspire better approach to this problem.

#### ACKNOWLEDGEMENTS

Authors gratefully acknowledge financial support from the Ministry of Education, Youth and Sports of the Czech Republic under NPU I programme (project No. LO1210) and from the Czech Science Foundation (project No. GA 15-14829S).

#### REFERENCES

- [1] I. Jakubova, J. Senk, I. Laznickova. The influence of nitrogen in argon/nitrogen mixture on parameters of high-temperature device with electric arc. *Acta Polytechnica* **53**(2):179–184, 2013.
- [2] J. Heinz, J. Senk. Modelling of energy processes in intensively blasted electric arc. *Czechoslovak J Phys* **54**(C):C702–708, 2004. DOI:10.1007/BF03166474.

- [3] A. Farmer, G. Haddad. *Material Functions and Equilibrium Composition of argon and Nitrogen Plasma*. Csiro Division of Applied Physics, 1989.
- [4] S. Ramakrishnan, A. Stokes, J. J. Lowke. An approximate model for high-current free-burning arcs. *J Phys D: Appl Phys* **11**:2267–2280, 1978.  
DOI:10.1088/0022-3727/11/16/014.
- [5] J. Senk, I. Jakubova, I. Laznickova. Treatment of near-electrode regions in a simple model of blasted electric arc. In *Proceedings of EPE 2016*. To be published, 2016.
- [6] J. Lowke. A unified theory of arcs and their electrodes. *J Phys IV* **07**(C4):C4–283–C4–294, 1997.